Ceramide displaces cholesterol from lipid rafts and decreases the association of the cholesterol binding protein caveolin-1

Cuijuan Yu, Michail Alterman, and Rick T. Dobrowsky[1]

Department of Pharmacology and Toxicology, University of Kansas, Lawrence, KS 66045

Abstract **Addition of exogenous ceramide causes a significant displacement of cholesterol in lipid raft model membranes. However, whether ceramide-induced cholesterol displacement is sufficient to alter the protein composition of caveolin-enriched lipid raft membranes is unknown. Therefore, we examined whether increasing endogenous ceramide levels with bacterial sphingomyelinase (bSMase) depleted cholesterol and changed the protein composition of caveolin-enriched membranes (CEMs) isolated from immortalized Schwann cells. bSMase increased ceramide levels severalfold and decreased the cholesterol content of detergent-insoluble CEMs by 25–50% within 2 h. To examine the effect of ceramide on the protein composition of the CEMs, we performed a quantitative proteomic analysis using stable isotope labeling of cells in culture and matrix-assisted laser desorption ionization time-of-flight mass spectrometry. Although ceramide rapidly depleted lipid raft cholesterol, the levels of the cholesterol binding protein caveolin-1 (Cav-1) decreased by 25% only after 8 h. Importantly, replenishing the cells with cholesterol rapidly reversed the loss of Cav-1 from the CEMs. Ceramide-induced cholesterol depletion increased the association of 5′-nucleotidase and ATP synthase β-subunit with the CEMs but had a minimal effect on changing the abundance of other lipid raft proteins, such as flotillin-1 and G-proteins. These results suggest that the ceramide-induced loss of cholesterol from CEMs may contribute to altering the lipid raft proteome.**—Yu, C., M. Alterman, and R. T. Dobrowsky. **Ceramide displaces cholesterol from lipid rafts and decreases the association of the cholesterol binding protein caveolin-1.** ***J. Lipid Res.*** **2005.** 46: **1678–1691.**

Supplementary key words caveolae • proteomics • sphingolipid • Schwann cells • stable isotope labeling with amino acids in cell culture • SILAC

Caveolae and lipid raft domains are distinct but related regions of the plasma membrane that are enriched in cholesterol, sphingomyelin, and glycosphingolipids (1, 2). Whereas lipid raft domains are present in many, if not all, cells (3), caveolae are specialized, morphologically distinct lipid raft domains that require the cell-specific expression of the protein caveolin-1 (Cav-1) (4).

The integrity of lipid rafts is very dependent upon the presence of cholesterol (5). Relative to phospholipids, sphingolipids are more hydrophobic, undergo more hydrogen bonding, and tend to cluster within cell membranes (6). Moreover, the ability of cholesterol to pack tightly with saturated lipids is essential to promoting the liquid-ordered structure of lipid raft domains (6). The loss of cholesterol from caveolae by treatment with cholesterol-sequestering agents, through increased sterol oxidation, or by inhibiting its de novo synthesis leads to a more disordered state and the loss of raft-associated proteins. Indeed, because Cav-1 is a cholesterol binding protein, it is often used to monitor the loss of caveolar integrity after cholesterol displacement or depletion. Recent reports have provided evidence that ceramide production in raft model membranes and astrocytes causes a significant displacement of cholesterol from lipid raft membranes (7, 8). However, whether a ceramide-induced displacement of cholesterol can lead to changes in the protein composition of caveolin-enriched membranes (CEMs) is unknown.

The recent development of stable isotope labeling of cells in culture (SILAC) (9) has enabled a quantitative, hypothesis-driven assessment of changes in a single protein (10) as well as the unbiased, quantitative characterization of large proteomes (11). The basic premise of SILAC is that two populations of cells are grown in medium containing either unlabeled amino acids or an amino acid containing deuterium or ^{13}C substitutions. After a suffi-

Manuscript received 16 February 2005 and in revised form 12 April 2005.

Published, JLR Papers in Press, May 1, 2005.
DOI 10.1194/jlr.M500060-JLR200

Abbreviations: bSMase, bacterial sphingomyelinase; Cav-1, caveolin-1; CEM, caveolin-enriched membrane; dFCS, dialyzed fetal calf serum; MALDI-TOF MS, matrix-assisted laser desorption ionization time-of-flight mass spectrometry; MβCD, methyl-β-cyclodextrin; SC, Schwann cell; SILAC, stable isotope labeling with amino acids in cell culture.

[1] To whom correspondence should be addressed.
e-mail: dobrowsky@ku.edu

cient incubation period to completely incorporate the labeled amino acid into the cellular proteome, one population of the cells serves as a control and the other is subjected to treatment. Cell lysates are then prepared and mixed together in a 1:1 mass ratio based upon total protein concentration. The mixed lysates may then be subjected to an enrichment procedure (immunoprecipitation, organelle isolation) for a targeted analysis, or the entire lysate can be fractionated by electrophoresis before matrix-assisted laser desorption ionization time-of-flight mass spectrometry (MALDI-TOF MS) or nanoelectrospray ionization MS/MS. Because minimal differences exist in the ionization efficiency between the same peptide containing a labeled versus an unlabeled amino acid, the ratio of intensities of the labeled to the unlabeled tryptic peptide provides a quantitative assessment of changes in the relative abundance of the parental protein after experimental treatment.

In this study, immortalized Schwann cells (SCs) were labeled with L-arginine ([^{12}C]Arg) or [U-$^{13}C_6$]L-arginine ([$^{13}C_6$]Arg) and treated with bacterial sphingomyelinase (bSMase) to create ceramide-enriched lipid raft domains, and the cholesterol content and protein composition of these membranes were determined. Ceramide production markedly decreased the cholesterol content of CEMs, which was redistributed to noncaveolar membranes. Ceramide-induced cholesterol displacement was associated with a 25% decrease in the level of Cav-1, which was reversed by cholesterol replenishment. In contrast to Cav-1, bSMase treatment increased the association of 5′-nucleotidase with the CEMs but had little effect on other abundant lipid raft-associated proteins, such as flotillins and G-proteins. These results suggest that a ceramide-induced decrease in cholesterol may contribute to altering the protein composition of lipid rafts.

EXPERIMENTAL PROCEDURES

SC preparation and stable isotope labeling with amino acids

Sciatic nerves were dissected from postnatal day 2 or day 3 Sprague-Dawley rat pups and primary SCs were isolated as described (12). S16 cells are an immortalized SC line that was generated by repetitive passaging of primary SCs (13) and were a kind gift from Dr. D. Mikol (University of Michigan).

All cells were cultured in low-glucose DMEM that was custom prepared in 4 liter batches and conformed to Gibco DMEM number 12320, with the exception that L-arginine and L-leucine were omitted. The amino acid-deficient medium contained antibiotics and 10% dialyzed fetal calf serum (dFCS; Atlas Biologicals, Fort Collins, CO), and the addition of the necessary amino acids produced complete medium. In experiments not requiring stable isotopes, the medium was supplemented with L-leucine (d0-Leu), and [^{12}C]Arg by the addition of 100× stock solutions prepared in serum-free leucine,arginine-deficient DMEM. In experiments requiring the stable isotopes, the medium was supplemented with L-5,5,5-trideutero-leucine (d3-Leu; Sigma/Aldrich, St. Louis, MO) or [$^{13}C_6$]Arg (Cambridge Isotopes, Andover, MA) by the addition of 100× stock solutions prepared in serum-free leucine, arginine-deficient DMEM.

Isolation of CEMs

Cells were placed on ice, washed with ice-cold PBS, and scraped into ice-cold MBST buffer (50 mM MES, pH 6.5, 400 mM NaCl, 1% Triton X-100, and 1× Complete® Protease Inhibitors; Roche Diagnostics). The cells were homogenized with a tight-fitting Dounce homogenizer, and CEMs were isolated by discontinuous sucrose gradient centrifugation as described previously (14). The samples were centrifuged in a SW41 rotor (126,000 *g*) or an MLS-50 rotor (129,000 *g*) for 16–18 h at 4°C. For biochemical analysis of protein distribution, 10 × 0.5 ml fractions were collected from the top of the gradients. After SDS-PAGE, the proteins were transferred to nitrocellulose and the membrane was stained with 0.5% Ponceau S in 5% trichloroacetic acid to visualize total protein. For immunoblot analysis, the membrane was typically cut in half and the upper half of the blot was used to probe for flotillin-1 (BD Signal Transduction Laboratories, Lexington, KY). The lower half of the blot was used to probe for Cav-1 (N-20 antibody; Santa Cruz Biotechnology, Santa Cruz, CA). Proteins were visualized using enhanced chemiluminescence (Amersham Biosciences, Piscataway, NJ).

Sphingomyelin, ceramide, and cholesterol measurements

Cellular sphingomyelin pools were labeled with 0.5 μCi/ml [^{3}H]choline (American Radiolabeled Chemicals, St. Louis, MO) for 3 days. The medium was removed, and the cells were washed with ice-cold PBS and placed in serum-free DMEM for 2 h before treatment with 100 mU/ml *Staphylococcus aureus* bSMase (Sigma/Aldrich) for 2–8 h. These short incubations with bSMase did not induce any substantial decrease in cell number or increase in trypan blue permeability (data not shown). CEMs were prepared as described above, and the lipids were extracted from aliquots of the gradient fractions (15). The extent of sphingomyelin hydrolysis and ceramide production was quantified by thin-layer chromatography and the diacylglycerol kinase assay, respectively (16).

To assess the effect of ceramide production on cholesterol levels, aliquots of the individual gradient factions were used directly in the Amplex Red cholesterol assay as described by the manufacturer (Molecular Probes, Eugene, OR); the Amplex Red cholesterol assay has a linear detection range of 0.05–10 μM cholesterol. To replenish cholesterol levels of the CEMs, the cells were treated for 1 h with a cholesterol-methyl-β-cyclodextrin (MβCD) complex (17). Six milligrams of cholesterol (Avanti Polar Lipids, Alabaster, AL) was resuspended in 0.08 ml of isopropanol-chloroform (2:1), and the lipid solution was added dropwise to 200 mg of MβCD in 2.2 ml of PBS at 80°C with stirring. The resulting clear solution was diluted into cell culture medium 100-fold, giving a final cholesterol concentration of ~70 μM. Preliminary experiments indicated that 1 h of incubation with the cholesterol-MβCD complex was sufficient to replenish caveolar cholesterol to at least control levels. In some experiments, cells were treated with 5 mM MβCD for 2 h to deplete caveolar cholesterol.

Quantitative proteomic analysis of CEMs by MALDI-TOF MS

S16 cells were cultured in medium containing either [^{12}C]Arg or [$^{13}C_6$]Arg (8–10 100 mm dishes each) and served as the control and experimental populations, respectively. The cells were treated with PBS or bSMase for 2–8 h as described above and scraped into ice-cold MBST. The protein concentration was measured in quadruplicate for each sample using the Coomassie blue binding assay and BSA as the standard (Bio-Rad, Hercules, CA). If necessary, protein measurements were repeated so that the coefficient of variation for the protein measurements was <5% for each sample. The lysates were then mixed in a 1:1 mass ratio and typically yielded 10–12 mg of total protein. CEMs were prepared, and the visible material concentrated at the interface

of the 5% and 35% sucrose layers was collected. The protein was diluted with 20 volumes of 50 mM MES, pH 6.5, 400 mM NaCl, and the membranes were collected by centrifugation at 100,000 *g* for 1 h at 4°C. The proteins of the isolated CEMs were then resolved by SDS-PAGE.

After SDS-PAGE, the gel was stained with colloidal Coomassie blue, and the bands were excised, chopped into small pieces, and placed in a silanized 0.6 ml microcentrifuge tube. The proteins were reduced and alkylated essentially as described to prepare for in-gel digestion (18). The dehydrated gel pieces were rehydrated on ice in a minimal volume of 12.5 ng/μl Trypsin Gold (Promega Corp., Madison, WI) in 25 mM ammonium bicarbonate, pH 7.5. A sufficient volume of 25 mM ammonium bicarbonate, pH 7.5, was added to cover the gel particles, and the proteins were digested overnight at 37°C. The supernatant was transferred to a fresh tube, and the peptides were extracted from the gel particles with 5% formic acid in 100 mM ammonium bicarbonate. The combined supernatants were desalted with C-18 Zip-tips (Millipore Corp., Billerica, MA) and eluted onto the MALDI sample plate with 10 mg/ml α-cyano-carboxycinnamic acid in 50% acetonitrile/0.1% trifluoroacetic acid. Acetonitrile, formic acid, and ammonium bicarbonate were of the highest grade obtainable and were purchased from Fisher Scientific (Pittsburgh, PA).

Samples were analyzed by MALDI-TOF MS using an Applied Biosystems Voyager-DE STR or a 4700 Proteomics Analyzer MALDI-TOF/TOF MS/MS instrument. The instruments were operated in the positive reflector mode at the following parameters: accelerating voltage, 20,000 V; grid voltage, 75%; mirror voltage ratio, 1:12; guide wire, 0.002%; extraction delay time, 180 ns. Acquisition mass range was 700–3,000 Da, and internal mass calibration was performed using the trypsin autolysis peaks (MH^+ 842.5021 and 2,211.0968). Protein identification was achieved after MALDI-TOF MS or MALDI-TOF/TOF MS/MS analysis by searching the mass data against the Swiss-Prot human and rodent databases using the Mascot search engine. For protein identification by peptide mass fingerprinting, search parameters used a peptide mass tolerance of 50 ppm, up to one missed cleavage, and carboxyamidomethylated cysteine as a fixed modification. Variable modifications were set to consider methionine oxidation and the presence of [$^{13}C_6$]Arg. Identification was considered positive when the molecular weight search (MOWSE) score indicated that the probability of identification was $P < 0.05$. All spectra were further verified by manual inspection. For peptide quantification, the peak height ratios or peak area ratios were calculated using values obtained from Applied Biosystems Data Explorer software (version 4.5). Similar results were obtained using either set of values.

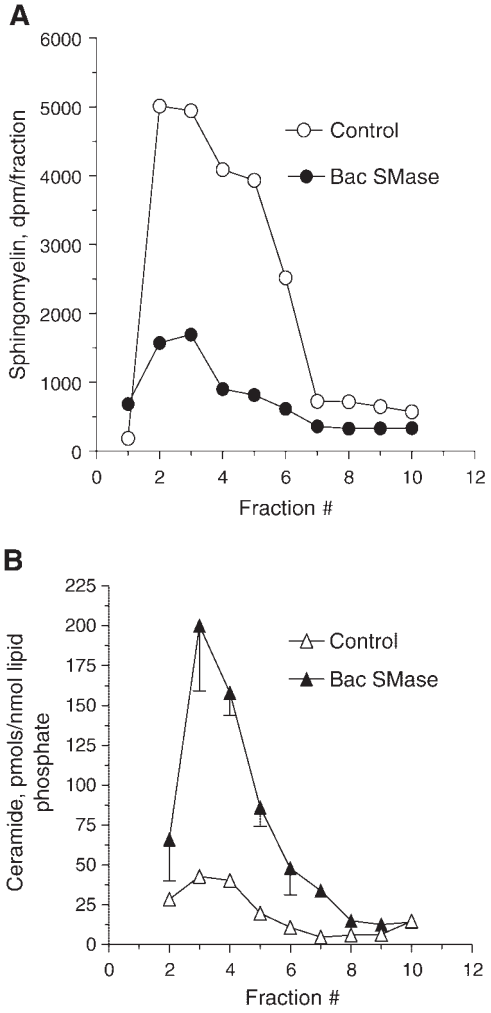

Fig. 1. Bacterial sphingomyelinase [bSMase (Bac SMase)] decreases sphingomyelin and increases ceramide levels in caveolin-enriched membranes (CEMs) isolated from S16 cells. A: S16 cells were labeled with [^{3}H]choline chloride for 3 days and treated with buffer or 100 mU/ml bSMase for 1 h. CEMs were isolated from equal amounts of protein, the lipids were extracted from each gradient fraction, and sphingomyelin was quantitated. B: S16 cells were treated with buffer or 100 mU/ml bSMase for 2 h. The CEMs were isolated from equal amounts of protein, and ceramide was quantified in each fraction. Ceramide levels were normalized to phospholipid phosphate and are presented as means ± SEM from three treatments.

RESULTS

Ceramide production in CEMs is associated with cholesterol depletion

bSMase is a convenient tool to increase cellular ceramide levels because the enzyme readily hydrolyzes sphingomyelin on the outer leaflet of the plasma membrane. S16 cells were treated with bSMase, and CEMs were isolated from equal amounts of protein. As anticipated, bSMase extensively hydrolyzed the sphingomyelin that localized to the CEMs (gradient fractions 2–4) of the S16 cells within 1 h (**Fig. 1A**); longer incubations had no additional effect on decreasing sphingomyelin levels. Concomitant with the hydrolysis of sphingomyelin, bSMase increased the mass of ceramide in the CEMs from 111.8 to 423.8 pmol/nmol phospholipid phosphate (Fig. 1B). These results demonstrate that bSMase effectively produces ceramide-enriched CEMs in S16 cells.

To examine the effect of ceramide generation on the cholesterol content of the CEMs, the cells were treated with bSMase for 2 h, CEMs were isolated from equal amounts of protein, and the total nanomoles of cholesterol and ceramide per gradient fraction was determined. bSMase increased the total amount of ceramide in the CEMs from a baseline value of 1.4 to 3.9 nmol (**Fig. 2A**). The increase in ceramide correlated with a loss of 49.3 ± 9.5 nmol of cholesterol, a 25% decrease from control values. The decrease in cholesterol from the CEMs was not

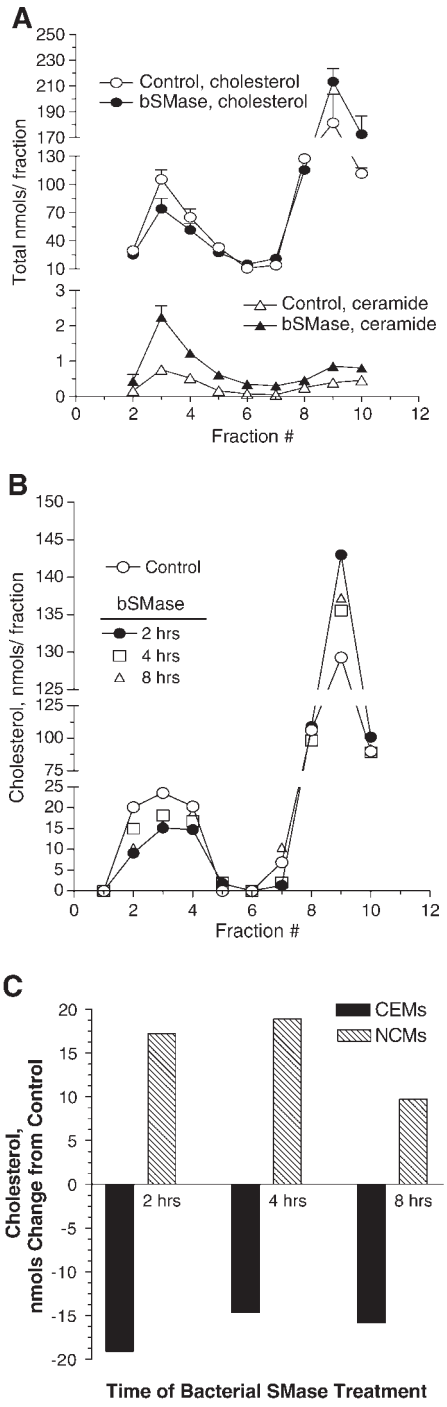

Fig. 2. Ceramide production is associated with a decrease in the cholesterol content of CEMs. A: Three confluent dishes of S16 cells were treated with buffer or 100 mU/ml bSMase for 2 h and the CEMs were isolated from equal amounts of protein. Total nanomoles of cholesterol and ceramide were quantified in each gradient fraction. Results shown are means ± SEM from two experiments performed in duplicate. B: Two confluent dishes of S16 cells were treated with buffer or 100 mU/ml bSMase for 2–8 h. CEMs were prepared as described above, and the cholesterol content of each gradient fraction was measured. Total cholesterol recovery from each treatment was as follows: control, 381 nmol; 2 h, 395 nmol; 4 h, 378 nmol; 8 h, 393 nmol. Results are from a single gradient and are representative of those obtained in three experiments. C: The difference between total nanomoles of cholesterol present in the CEMs (gradient fractions 2–4) and noncaveolar membranes (NCMs; gradient fractions 8–10) of control and bSMase-treated cells was calculated from the data in B.

attributable to differences in sterol recovery because the total nanomoles of cholesterol present in the gradient was similar between control (679.6 nmol) and bSMase-treated (694.8 nmol) cells. Indeed, results in Fig. 2B, C show that over 2–8 h of bSMase treatment, the loss of cholesterol from the CEMs was recovered in noncaveolar membranes (fractions 8–10), representing organellar and bulk plasma membranes. Importantly, this effect was reversible, because cholesterol levels in the CEMs were readily replenished after incubation with the cholesterol-MβCD complex for 1 h (data not shown, but see Fig. 8B). Because cholesterol is much more abundant in the CEMs than ceramide, these data suggest that ceramide may be very effective at displacing the sterol from these lipid raft domains.

SILAC as an analytical approach in primary and immortalized SCs

SILAC offers a useful quantitative approach to determine whether the ceramide-induced loss of cholesterol was sufficient to cause changes in the proteome of the CEMs. A critical parameter for accurate quantitation by SILAC is that one population of cells completely incorporates a labeled amino acid into its proteome (19). This can be readily achieved as the cells undergo multiple population doublings. However, the presence of unlabeled amino acids in FCS can compete with the isotopically labeled amino acid and lead to a mixture of labeled and unlabeled amino-acyl tRNAs that both contribute to protein synthesis. Although the use of dFCS avoids this problem (9), some cells require low molecular weight serum components for growth that are also removed by dialysis (20). Because SILAC analysis has not been performed on primary or immortalized SCs, it was necessary to assess the ability of these cells to grow in dFCS and incorporate heavy amino acids into their proteomes. Primary SCs retained their overall cell morphology and viability in medium containing dFCS, but their growth rate was slightly slower compared with that of cells maintained in DMEM-10% FCS. Similarly, no substantial difference was observed in the growth or morphology of the immortalized S16 SCs in medium containing dFCS compared with medium supplemented with FCS (data not shown).

To validate that the primary SCs readily incorporated a heavy amino acid, we used d3-Leu because it is economical and is a rather abundant amino acid in most proteins. Primary SCs were grown in DMEM-10% dFCS containing d0-Leu or d3-Leu for 14 days, the cells were scraped into lysis buffer, and the protein lysates were mixed in a 1:1 mass ratio. After SDS-PAGE and staining of the gel, two abundant bands [identified as vimentin (52 kDa) and β-actin (42 kDa)] were excised and subjected to in-gel reduction, alkylation, and tryptic digestion. A strong benefit of SILAC is that the rapid identification of d3-Leu-containing peptides is facilitated by the presence of a characteristic doublet of peak clusters that differ in mass by the number of leucine residues in the peptide and multiplied by 3. **Figure 3A** shows a representative peak doublet for the labeled and unlabeled ^{171}LQEEMLQR^{178} peptides of vimentin. The presence of two leucine residues in the un-

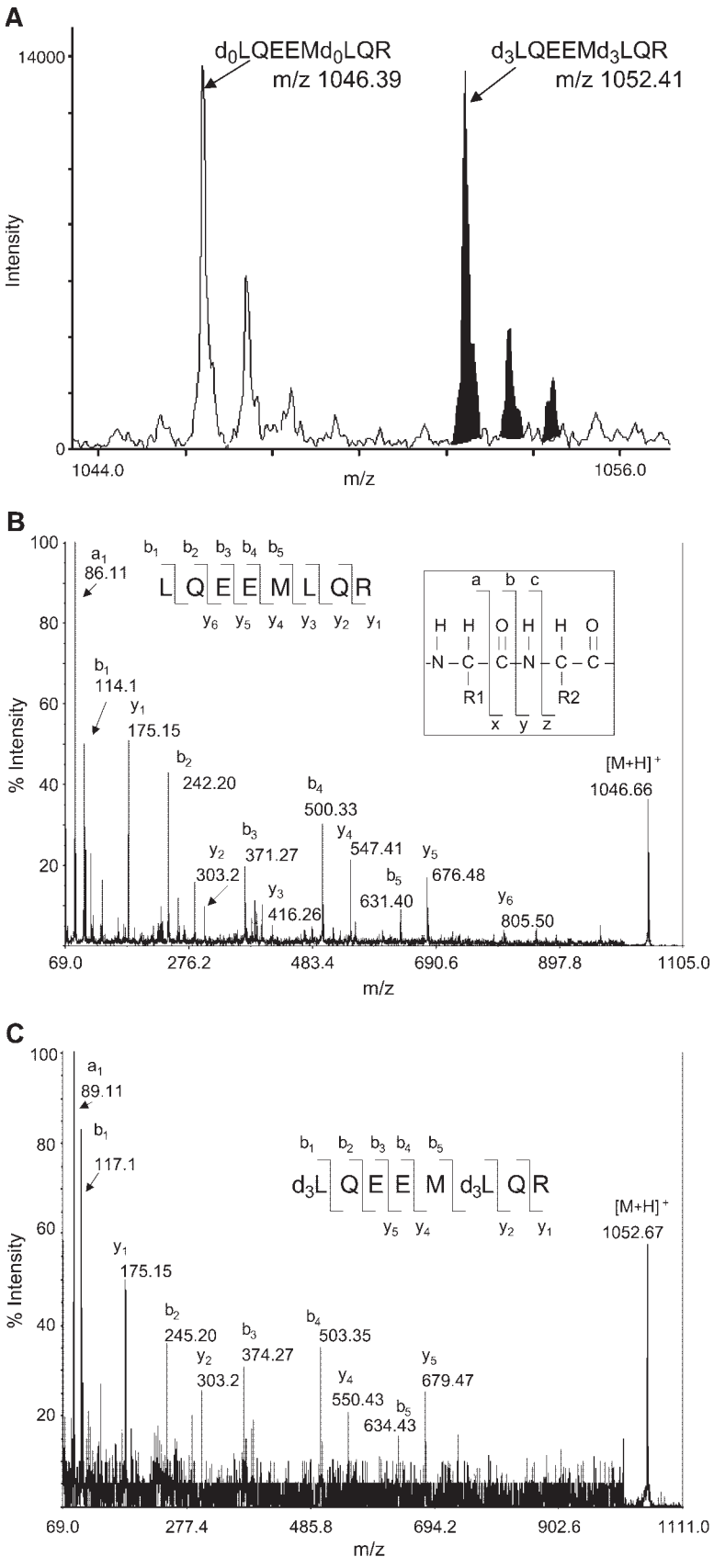

Fig. 3. Incorporation of L-5,5,5-trideutero-leucine (d3-Leu) into the Schwann cell (SC) proteome. Primary SCs were grown in medium supplemented with L-leucine (d0-Leu) or d3-Leu for 14 days. Cell lysates were prepared and mixed in a 1:1 mass ratio based upon total protein concentration, and the proteins were resolved by SDS-PAGE. The vimentin band (52 kDa) was excised and digested with trypsin, and the peptides were analyzed by matrix-assisted laser desorption ionization time-of-flight mass spectrometry (MALDI-TOF MS). A: The MS spectrum shown is an expanded scale from the peptide mass fingerprint of vimentin to clearly show the presence of a peptide doublet produced from equivalent amounts of labeled and deuterated peptide. B: MALDI-TOF/TOF MS/MS of the peptide at *m/z* 1046.66. The inset shows the nomenclature for ions produced by differential fragmentation of the peptide bond. C: MALDI-TOF/TOF MS/MS of the peptide at *m/z* 1052.67.

labeled peptide (*m/z* 1,046.39) results in a shift in the mass of the d3-Leu-containing peptide by 6 Da (*m/z* 1,052.41). The peaks at *m/z* 1,047.39 and 1,048.39 (1,053.41 and 1,054.41 in the d3-Leu peptide) form the isotope cluster of the peptide. These peaks arise from the 1% probability that the natural abundance of the ^{13}C isotope replaces any ^{12}C atom in the unlabeled peptide (21). We verified that these doublets represent actual d0-Leu and d3-Leu peak

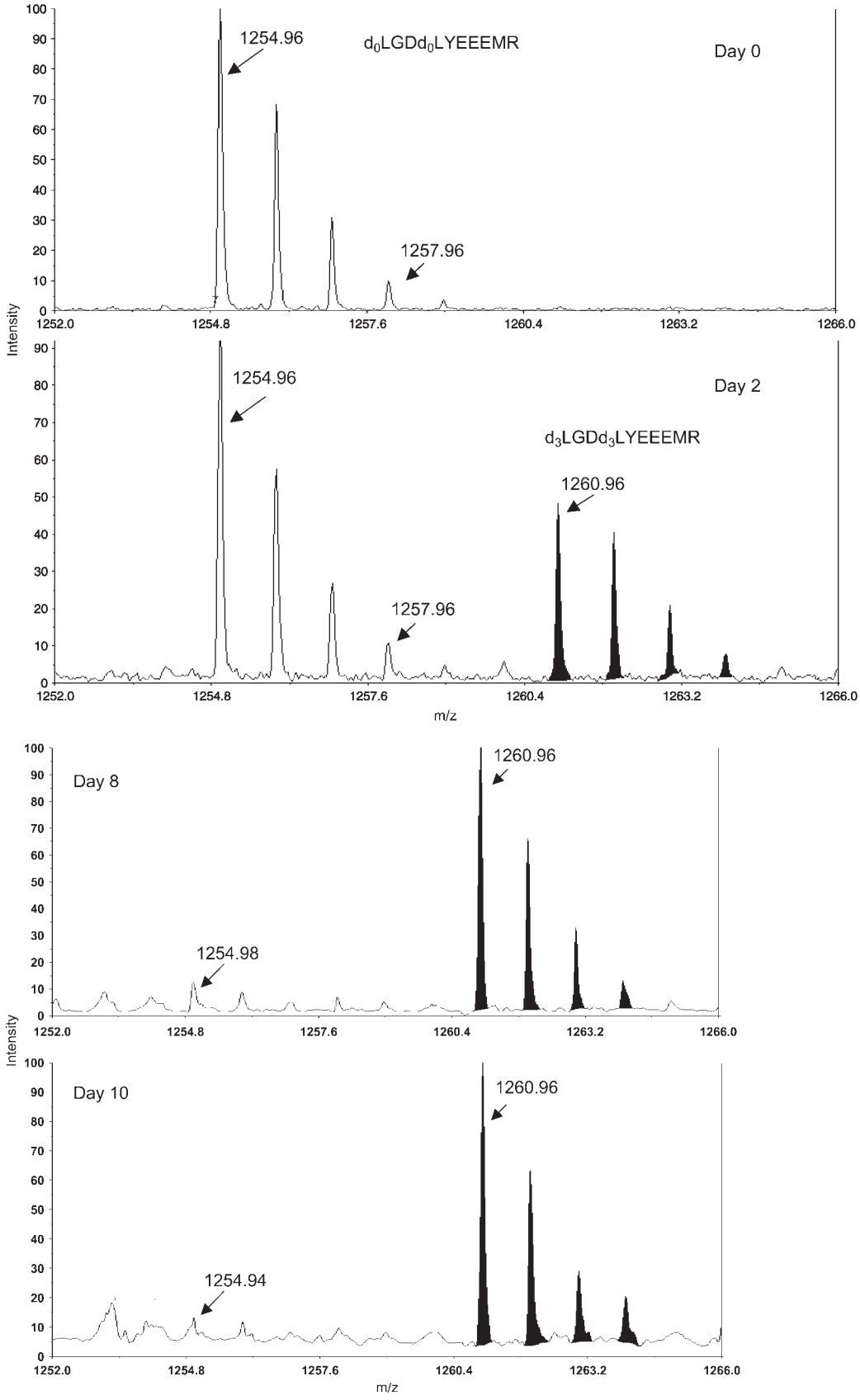

Fig. 4. Kinetics of d3-Leu incorporation into the SC proteome. Primary SCs were grown to confluence in medium supplemented with d0-Leu (day 0) and then subcultured in medium supplemented with d3-Leu. The cells were grown without further subculturing, and cell lysates were prepared on the indicated days. The proteins were resolved by SDS-PAGE, the vimentin band was excised and digested, and the peptides were analyzed by MALDI-TOF MS. As d0-Leu is replaced in the proteome with d3-Leu, the abundance of the d0-Leu-containing peptide (unshaded peaks) decreases while the deuterated peptide increases (shaded peaks).

clusters by MALDI-TOF/TOF MS/MS. The precursor mass window of ±1.0 Da was centered on the most abundant isotopomers of the peptide doublet, and MS/MS fragmentation of the peptide bonds produced an extensive series of b-ions and y-ions of the unlabeled (Fig. 3B) and deuterated (Fig. 3C) peptides. The resulting peptide sequence tags provided definitive identification of this vimentin peptide and the location of the d3-Leu residues. For example, leucine is at the N terminus of this peptide. This is supported by the entire series of b-ions (b_1 to b_5) that were shifted by 3 Da in the deuterated species and by the presence of a_1-ions at *m/z* 86.11 and 89.13 for d0-Leu and d3-Leu, respectively. Similarly, the observed y_4- and y_5-ions (but not the y_1- and y_2-ions) also showed a shift of 3 Da, consistent with the presence of d3-Leu as the sixth amino acid.

To determine the minimal time necessary for complete incorporation of d3-Leu into the SC proteome, we as-

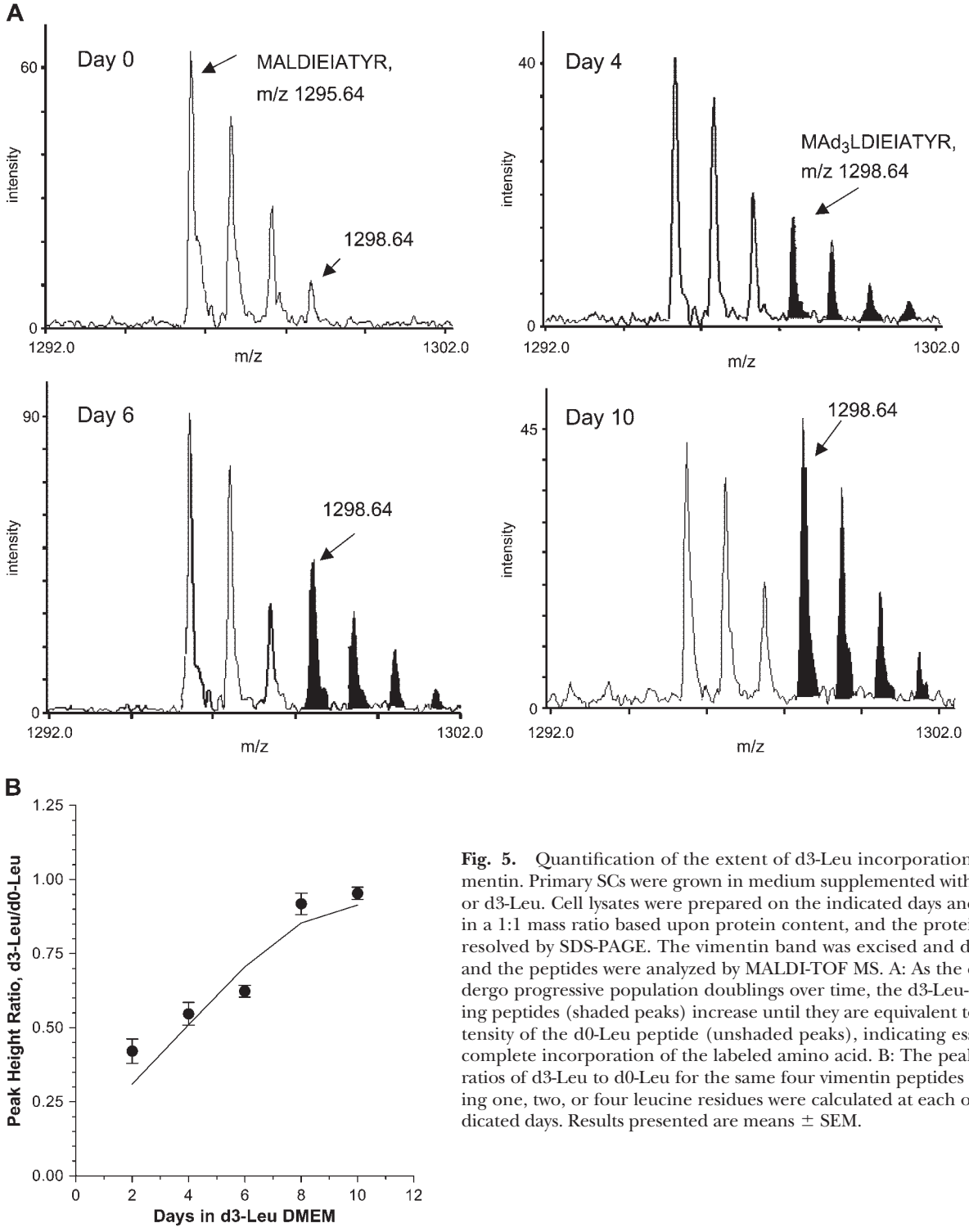

Fig. 5. Quantification of the extent of d3-Leu incorporation into vimentin. Primary SCs were grown in medium supplemented with d0-Leu or d3-Leu. Cell lysates were prepared on the indicated days and mixed in a 1:1 mass ratio based upon protein content, and the proteins were resolved by SDS-PAGE. The vimentin band was excised and digested, and the peptides were analyzed by MALDI-TOF MS. A: As the cells undergo progressive population doublings over time, the d3-Leu-containing peptides (shaded peaks) increase until they are equivalent to the intensity of the d0-Leu peptide (unshaded peaks), indicating essentially complete incorporation of the labeled amino acid. B: The peak height ratios of d3-Leu to d0-Leu for the same four vimentin peptides containing one, two, or four leucine residues were calculated at each of the indicated days. Results presented are means ± SEM.

sessed the kinetics of its uptake. Primary SCs were grown in DMEM-10% dFCS and 2 μM forskolin containing d0-Leu (day 0), then subcultured in the same medium containing d3-Leu for 2–10 days. At the indicated day, the cells were scraped into lysis buffer and the proteins were resolved by SDS-PAGE. The vimentin band was excised and processed for MALDI-TOF MS analysis. **Figure 4** shows the progressive incorporation of d3-Leu into the ^{128}LGDLYEEEMR^{137} peptide of vimentin. As described above, the presence of two leucine residues shifts the mass of the deuterated peptide by 6 Da (*m/z* 1,254.96 to 1,260.96). As expected at day 0, the absence of a peak at *m/z* 1,260.96 indicates that no deuterated peptide is present. After 2 days in medium containing d3-Leu, the ratio of the peak at *m/z* 1,260.96 to the unlabeled peptide at *m/z* 1,254.96 indicates that the extent of incorporation was ~45–50%. Importantly, any increase in the intensity of the isotopomer at *m/z* 1,257.96 would indicate the presence of a monodeuterated species. However, the abundance of this peak did not increase relative to that present in unlabeled cells (day 0). This indicates that d3-Leu has effectively saturated the leucine-tRNA pool and that d3-Leu present in the medium is the primary source of this amino acid for new protein synthesis. By day 8, the unlabeled peptide accounted for <10% of the mass, and it was essentially lost after 10 days of incubation in medium containing d3-Leu. Similar results were obtained when lysates from cells grown in either d0-Leu or d3-Leu for various times were mixed on an equal mass basis. In this approach, complete incorporation of the d3-Leu was also evident by 10 days, because the ratio of unlabeled to labeled peptide reaches unity (**Fig. 5A**).

To provide an estimate of the variability associated with d3-Leu incorporation, the ratio of d3-Leu to d0-Leu from vimentin peptides containing one, two, or four leucine residues (four peptides per time point) was quantified. Theoretically, if the labeled amino acid is the only available source for protein synthesis, then >97% of the d3-Leu should become incorporated into proteins after five population doublings (1–0.5^5) (9). Because the primary rat SCs undergo a population doubling every 40–48 h in the low-glucose DMEM-10% dFCS, 10 days is equivalent to five to six population doublings. In good agreement with the theoretical prediction, the incorporation of d3-Leu was 95.4 ± 2.1% after 10 days in the labeled medium (Fig. 5B). It is important to note that one limitation of using d3-Leu is that the isotope distributions in peptides containing only one leucine residue may overlap. For example, the peak at *m/z* 1,298.64 in Fig. 5A is present in the unlabeled peptide at day 0, and the incorporation of one d3-Leu increases the intensity of this peak. Therefore, to obtain the correct quantitative estimate of the deuterated peptide, it is necessary to subtract this baseline contribution from the unlabeled isotopomer using an isotope correction factor. This is readily performed using the MS-Isotope tool of Protein Prospector but can be avoided using other labeled amino acids, as discussed below.

Relative protein quantification by SILAC

To establish some analytical limits for quantitation by SILAC using MALDI-TOF MS, we measured changes in known mixtures of unlabeled and labeled proteins that varied over a range of 25–400%. Cells were grown in d0-Leu or d3-Leu for 10 days, and the lysates were mixed to give various theoreti-

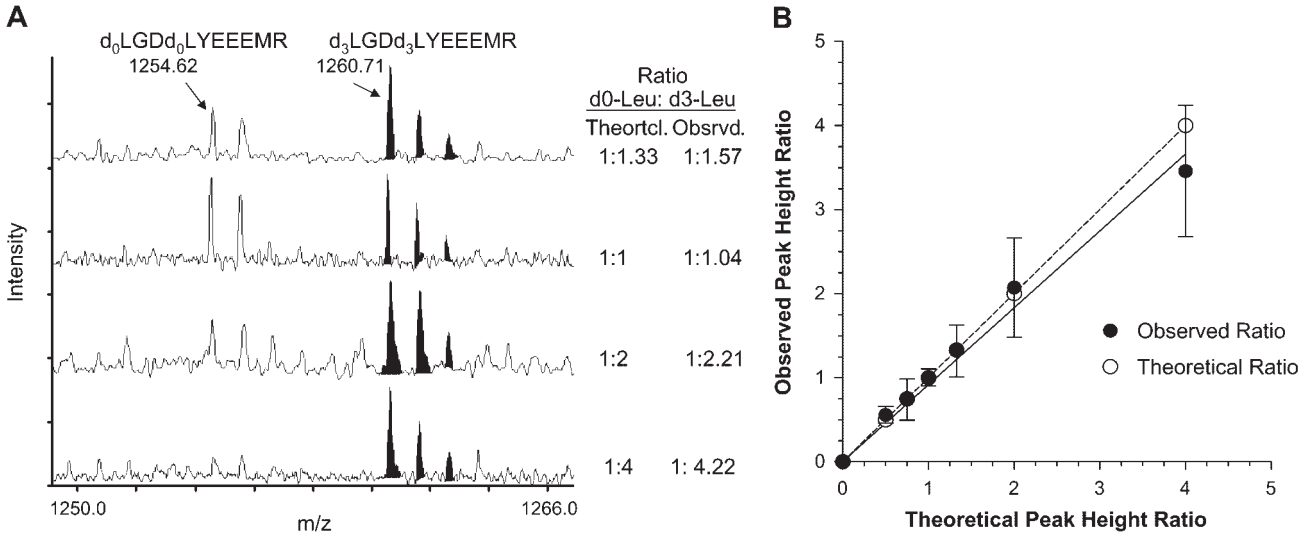

Fig. 6. Determination of the linearity of quantitation by stable isotope labeling with amino acids in cell culture. Primary SCs were grown in medium supplemented with d0-Leu or d3-Leu for 10 days. Cell lysates were prepared and mixed in varying ratios based upon protein concentration to give standard mixtures containing the indicated theoretical ratios of unlabeled to labeled protein. The proteins were resolved by SDS-PAGE, the vimentin band was excised and digested, and the peptides were analyzed by MALDI-TOF MS. A: Annotated peaks show representative spectra obtained for the indicated theoretical (Theortcl) ratios of d0-Leu (unshaded) to d3-Leu (shaded) peptides. The observed (Obsrvd) peak height ratio for each spectrum is shown. B: The observed peak height ratios were calculated for six vimentin peptides containing one, two, or four leucine residues in each of six standard mixtures. Linear regression analysis was performed to establish the relationship between the predicted versus observed peak height ratios. Results presented are means ± SEM.

cal mass ratios of d0-Leu to d3-Leu (1:0.5, 1:0.75, 1:1, 1:1.33, 1:2, and 1:4). An aliquot of each mixture was subjected to SDS-PAGE, and the vimentin bands were analyzed by MALDI-TOF MS. The observed ratios of nondeuterated-to-deuterated peptide were typically within 10% of the theoretical ratios, with the exception of the standard mixture at a ratio of 1:1.33 (**Fig. 6A**). However, upon averaging of the observed peak height ratios of the deuterated-to-nondeuterated peptides over six doublets that contained one, two, or four leucine residues in each of the six mixtures, there was very good agreement with the expected theoretical ratios (Fig. 6B). Although the linearity of the response began to deviate in the quantitation of greater fold differences, this was not attributable to signal saturation in the mass spectrometer. These data suggest that we may underestimate peptides changing by 4-fold or greater. Although we have not directly identified the source of this error, it may arise at least in part from a greater percentage contribution to the signal intensity from background noise in the unlabeled sample.

Although leucine is the most abundant essential amino acid in proteins, its use in SILAC can be problematic. As mentioned, it is necessary to perform isotope corrections for peptide doublets containing a single leucine residue. Additionally, leucine may not be present in the limited number of peptides produced by tryptic digestion of low molecular weight proteins. Because trypsin cleaves specifically at lysine and arginine residues (22), the use of [$^{13}C_6$]Arg for protein labeling *1*) produces numerous doublets that all differ by 6 Da (unless an arginine is followed by a proline), *2*) increases the number of peptide doublets available for quantitation, *3*) avoids the need to correct for isotopic contributions from the unlabeled partner of most peptide doublets, and *4*) increases the confidence of protein identification (if the search results attribute a doublet peak containing [^{13}C]Arg to a peptide ending in lysine, it is likely an incorrect assignment). Therefore, [^{13}C]Arg was used in the remaining experiments.

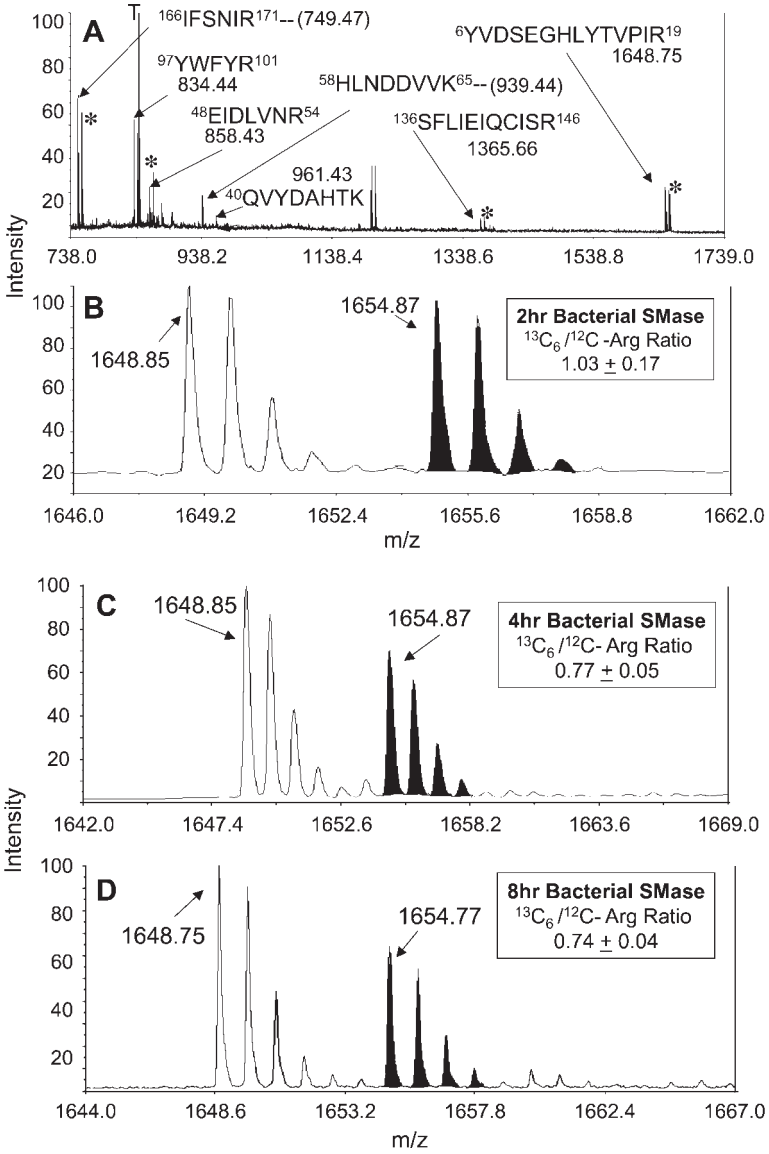

Fig. 7. bSMase treatment decreases the association of caveolin-1 (Cav-1) with CEMs. A: Peptide mass fingerprint of Cav-1 isolated from a 1:1 mixture of L-arginine/[U-$^{13}C_6$]L-arginine ([^{12}C]Arg:[$^{13}C_6$]Arg)-labeled CEMs. The spectrum shows five arginine-containing peptide doublets and two lysine peptides that do not appear as doublets. The mass of the indicated [^{12}C]Arg peptides is given, and the asterisks indicate the [$^{13}C_6$]Arg peaks (the [$^{13}C_6$]Arg peak for 840.44 is not shown). The base peak in the spectrum at *m/z* 842.51 is from trypsin (T), and the peptide doublet at *m/z* 1,204.33 is from an unidentified comigrating protein. B–D: The cells were treated with buffer ([^{12}C]Arg) or 100 mU/ml bSMase ([$^{13}C_6$]Arg) for 2–8 h, and Cav-1 was quantified by MALDI-TOF MS. The expanded mass scale shows the changes in the [^{12}C]Arg (*m/z* 1,648.8; unshaded):[$^{13}C_6$]Arg (*m/z* 1,654.8; shaded) doublet as representative of all arginine-containing Cav-1 peptide doublets at each time point. The peak area ratios for all of the Cav-1 peptide doublets at each time point were calculated and are shown in the insets as means ± SEM.

Effect of bSMase on the protein profile of CEMs from S16 cells

S16 cells are an immortalized line of rat SCs that undergo rapid population doubling compared with primary SCs. Although the S16 cells readily incorporated [$^{13}C_6$]Arg to a sufficient level within 5 days (data not shown), they were maintained upon subculturing in medium supplemented with [$^{13}C_6$]Arg for 20–30 passages. Under these conditions, the level of incorporation of the label should theoretically exceed 99.99%. S16 cells were treated with buffer ([^{12}C]Arg) or 100 mU/ml bSMase ([$^{13}C_6$]Arg) for 2–8 h, and cell lysates were prepared. After mixing the lysates in a 1:1 mass ratio, CEMs were isolated and the proteins were resolved by SDS-PAGE and prepared for analysis by MALDI-TOF MS.

Cav-1 is a cholesterol binding protein (23) whose association with CEMs is decreased upon depleting cellular cholesterol with cholesterol binding agents such as MβCD (24). **Figure 7A** shows a representative peptide mass fingerprint for rat Cav-1. Evident is the presence of five [^{12}C]Arg:[$^{13}C_6$]Arg peptide doublets that aided both quantification and identification. Indeed, **Table 1** shows that, on average, five [^{12}C]Arg:[$^{13}C_6$]Arg tryptic peptide doublets were used for quantification versus 9–10 total tryptic peptides ([^{12}C]Arg- + [$^{13}C_6$]Arg- + [^{12}C]lysine-containing peptides) that facilitated identification.

Surprisingly, despite the substantial decrease in caveolar cholesterol within 2 h of bSMase treatment, no change in Cav-1 was observed by SILAC analysis (Fig. 7B). However, Cav-1 levels decreased progressively by 20–25% after 4–8 h of bSMase treatment (Fig. 7C, D). To complement the results of the MS analysis, immunoblot analysis for Cav-1 was also performed. In good agreement with the SILAC analysis, densitometry of the immunoblots indicated that bSMase treatment for 8 h decreased Cav-1 by ~25% (**Fig. 8A**). Importantly, replenishing cholesterol for 1 h, after 7 h of treatment with bSMase, reversed the loss of Cav-1 (Fig. 8B). These results support the notion that the loss of Cav-1 from the CEMs was associated with the ceramide-induced cholesterol depletion. In contrast, bSMase treatment did not substantially alter the level of G-proteins, flotillin-1, and flotillin-2 (**Table 2**, Fig. 8A), which undergo a substantial decrease in lipid rafts after cholesterol depletion by MβCD (25). Indeed, the G-protein, Gi-α3, was substantially depleted from the CEMs after 2 h of treatment with 5 mM MβCD but was essentially unchanged by bSMase treatment (**Fig. 9**). On the other hand, prolonged incubation with bSMase induced a 50% increase in 5′-nucleoti-

TABLE 1. Representative results for the number of peptides used for protein identification versus protein quantitation by stable isotope labeling with amino acids in cell culture and matrix-assisted laser desorption ionization time-of-flight mass spectrometry analysis

Protein	Swiss-Prot Accession Number	Number of Peptides Quantitated	Number of Peptides in Identification	Percent Coverage
Caveolar proteins				
Caveolin-1	P49817	5	8	44
Flotillin-1	Q9Z1E1	10	18	26
Flotillin-2	Q9Z2S9	3	6	17
G-β1 subunit	P04901	4	5	20
G-β2 subunit	P11016	7	8	26
Gi-α1 subunit	P10824	2	7	16
Gi-α2 subunit	P04897	8	15	45
Gi-α3 subunit	P08753	6	10	27
Go-α2 subunit	P30033	3	8	23
		5.3	**9.4**	**27.1**
Noncaveolar proteins				
B cell receptor-associated protein 37	O35127	4	8	29
β-Actin	P60711	7	9	31
Histone 2A.1	P02262	2	3	27
Histone 2B	Q00715	2	3	24
Histone H4	P02304	3	5	50
HSP 90-β	P08238	3	6	9
Myosin I β	Q9WTI7	21	46	26
O-Acetyl GD3 ganglioside synthase	P70490	7	9	20
Phosphopantothenate-cysteine ligase	Q9HAB8	3	7	24
Rap-1b	P09526	2	4	25
Rap-2a	P10114	2	4	21
Tubulin α-6 chain	P05216	3	4	11
VDAC-1	Q9Z2L0	1	8	38
Vimentin	P31000	11	24	32
V-ATPase subunit A	P38607	2	4	7
V-ATPase subunit B2	P50517	3	6	11
V-ATPase subunit E	P50518	3	6	30
		4.9	**9.7**	**26.4**

Variable search parameters for protein identification included methionine oxidation and [$^{13}C_6$]arginine. Peptides containing methionine oxidation were not included in the number of peptides used for identification or quantification if a nonoxidized peptide was also detected. Percent coverage was obtained directly from the Mascot search results. Boldface numbers are averages for each column.

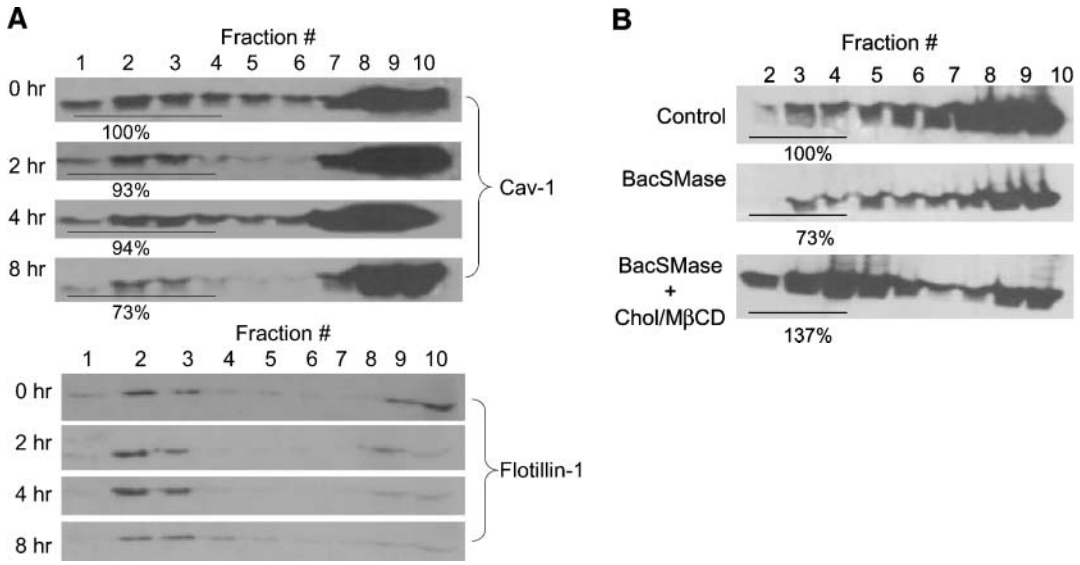

Fig. 8. Replenishing cholesterol reverses the loss of Cav-1 from CEMs after treatment with bSMase. A: S16 cells were treated with buffer or 100 mU/ml bSMase for the indicated times, CEMs were isolated, and aliquots of the individual gradient fractions were subjected to SDS-PAGE. Immunoblot analysis for Cav-1 (upper panels) or flotillin-1 (lower panels) was performed after cutting the blot at the 37 kDa molecular mass marker. B: S16 cells were treated for 8 h with buffer or 100 mU/ml bSMase (BacSMase), and the cholesterol-methyl-β-cyclodextrin (Chol/MβCD) complex was added for the final hour in one of the incubations with bSMase. CEMs were isolated, and aliquots of the individual gradient fractions were subjected to SDS-PAGE. Cav-1 was detected by immunoblot analysis.

dase, a well-established raft protein (25), and an ~50% decrease in the recently identified raft protein ATP synthase-β chain (26).

DISCUSSION

Our results show that treatment of immortalized SCs with bSMase increased the ceramide content of the CEMs and correlated with a 25–50% decrease in the cholesterol level of the CEMs within 2 h. Additionally, the cholesterol content of the CEMs remained well below that present in untreated S16 cells even after 8 h in the presence of bSMase. Overall, these results closely agree with the 50% decrease in plasma membrane cholesterol after treatment of astrocytes (8) or 3T3-L1 preadipocytes with bSMase (27). In contrast to our results, however, cholesterol levels recovered within 3 h in the continued presence of bSMase in preadipocytes. Presumably, this difference may reflect the different concentrations of enzyme used, 1 mU/ml (27) versus 100 mU/ml in this study, or cell-specific events that control cholesterol synthesis and trafficking. Similarly, our data also agree with predictions based upon results from lipid raft model membranes. In lipid vesicles composed of both raft domains and disordered fluid domains, the addition of exogenous ceramide displaced cholesterol from the raft domains (7). In this regard, the loss of cholesterol from the CEMs correlated reasonably well with an increase in the cholesterol content of noncaveolar membranes, which consist of a mixture of bulk plasma membrane and organellar membranes. These data agree with a previous report indicating that the loss of plasma membrane cholesterol after bSMase treatment is not attributable to cholesterol efflux (28). However, we did not ascertain whether the displacement of cholesterol from the CEMs was associated specifically with esterification and the production of an internalized pool.

At this point, our study does not address how ceramide generation may displace cholesterol from lipid raft domains. The interaction of cholesterol with sphingomyelin occurs through hydrogen bonding of the C3-hydroxyl of cholesterol with the sphingosine backbone of sphingomyelin. Although this structure is maintained in ceramide, the loss of the polar phosphocholine group results in ceramide having a very poor affinity for cholesterol. Indeed, biophysical studies have shown that ceramides mix very poorly with cholesterol and spontaneously undergo lateral phase separation and the formation of a ceramide-enriched microdomain (29). Additionally, recent evidence also indicates that ceramide phosphoethanolamine, which lacks the three methyl groups of the phosphocholine head group present in sphingomyelin, does not interact favorably with cholesterol (30). These data strongly support the notion that the phosphocholine head group is also important for stabilizing sphingolipid-sterol interactions (30). Thus, although ceramides generated from sphingomyelin hydrolysis share the same sphingoid base and fatty acid composition, this is not sufficient to promote a cholesterol-ceramide interaction. Conceivably, as sphingomyelin is hydrolyzed, the production of ceramide-enriched microdomains creates a poor environment for cholesterol-sphingolipid interactions. Consistent with this possibility, SMase D was substantially less effective than SMase C at mobilizing free cholesterol, despite decreasing sphingomyelin levels to a similar extent (28). Because SMase D hydrolyzes sphingomyelin to ceramide-1-phosphate, this

TABLE 2. Quantitative proteomic analysis of the effect of bSMase treatment on proteins identified in caveolin-enriched membranes

Protein	Swiss-Prot Accession Number	Time of bSMase Treatment		
		2 h	4 h	8 h
Caveolar proteins				
ATP synthase β-chain	P10719	nd	0.84 ± 0.12	0.56 ± 0.19
Caveolin-1	P49817	1.03 ± 0.16	0.77 ± 0.05	0.74 ± 0.08
Flotillin-1	Q9Z1E1	1.15 ± 0.43	1.03 ± 0.29	1.2[a]
Flotillin-2	Q9Z2S9	0.92 ± 0.19	0.84 ± 0.12	1.01 ± 0.19
G-β1 subunit	P54311	0.93 ± 0.02	nd	0.92 ± 0.02
G-β2 subunit	P54313	0.89 ± 0.17	0.95 ± 0.16	1.00 ± 0.1
Gi-α2 subunit	P04897	0.87 ± 0.09	1.15 ± 0.11	1.04 ± 0.10
Gi-α3 subunit	P08753	0.79 ± 0.14	1.13 ± 0.11	0.91 ± 0.18
Go-α2 subunit	P30033	0.78 ± 0.11	0.99 ± 0.33	0.85 ± 0.29
5′-Nucleotidase	P21588	nd	0.96 ± 0.07	1.66 ± 0.44
Noncaveolar proteins				
β-Actin	P60711	1.12 ± 0.08	1.80 ± 0.13	1.06 ± 0.14
Histone H4	P02304	0.75 ± 0.04	1.18 ± 0.09	0.73 ± 0.04
O-Acetyl GD3 ganglioside synthase	P70490	0.72 ± 0.36	1.52 ± 0.07	nd
Tubulin α-6 chain	P05216	0.97 ± 0.39	nd	nd
Tubulin β-2 chain	P05217	nd	nd	0.88 ± 0.25
Tubulin β-15 chain	P04691	nd	nd	0.97 ± 0.20
V-ATPase subunit A	P50516	0.78[a]	nd	1.10 ± 0.42
V-ATPase subunit B	P62815	0.85 ± 0.10	1.37 ± 0.03	1.07 ± 0.22
V-ATPase subunit D	P51863	nd	0.96 ± 0.16	0.81 ± 0.13
V-ATPase subunit E	P50518	0.90 ± 0.07	nd	nd
VDAC-1	Q9Z2L0	0.79[a]	0.90 ± 0.04	0.94[a]
Vimentin	P31000	1.14 ± 0.16	1.64 ± 0.51	1.05 ± 0.26

bSMase, bacterial sphingomyelinase; nd, not detected. Results shown are peak area ratios of the total number of quantifiable peptide doublets in each protein and are presented as means ± SEM.

[a] Average of only two peptides available for quantitation.

phosphorylated ceramide derivative does not mimic the actions of ceramide in the raft domains. These results support the idea that cholesterol displacement is associated with increased ceramide production rather than the loss of sphingomyelin per se (28).

To facilitate characterizing the effect of ceramide-induced cholesterol depletion on the protein composition of the CEMs, we used a stable isotope labeling procedure that permits a quantitative proteomic analysis between two cell populations. SILAC has been used to provide both targeted (10, 31) and more global quantitative analyses of cellular proteomes (20, 25). We have documented the suitability of this approach using both primary SCs and immortalized S16 SCs. Primary SCs readily incorporated d3-Leu into the cellular proteome with essentially no effect on cell growth and viability. We have also used [$^{13}C_6$]Arg and [$^{13}C_9$]tyrosine to label primary SCs and have encountered no problems with incorporation of the labeled amino acids into the proteome (data not shown). As a secondary note, some cell lines can catabolize argi-

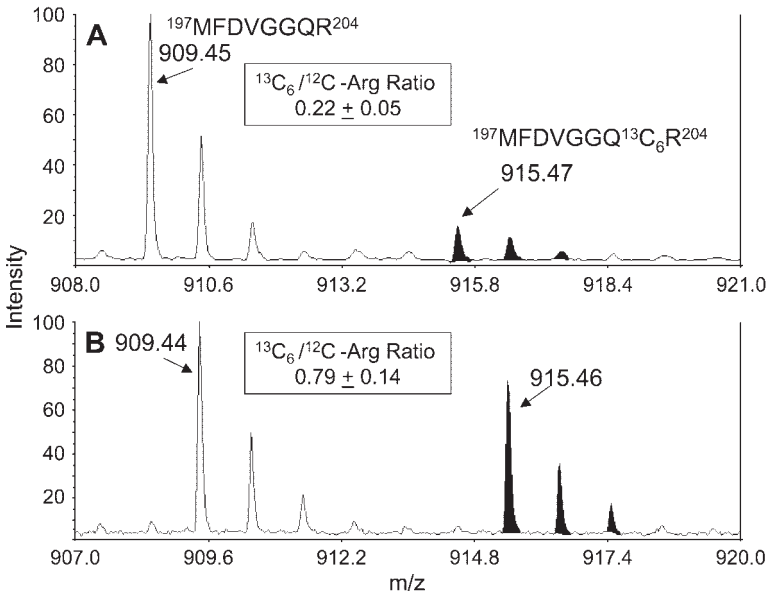

Fig. 9. Cholesterol depletion by MβCD leads to a prominent loss of G-proteins from CEMs. S16 cells were treated with buffer ([^{12}C]Arg), 5 mM MβCD ([$^{13}C_6$]Arg), or 100 mU/ml bSMase ([$^{13}C_6$]Arg) for 2 h. Cell lysates were prepared and mixed in a 1:1 ratio based upon total protein concentration, CEMs were isolated, and the proteins were resolved by SDS-PAGE. The bands corresponding to various G-protein family members (~40 kDa) were excised and digested, and the peptides were analyzed by MALDI-TOF MS. The expanded mass scale shows the changes in the [^{12}C]Arg (*m/z* 909.4; unshaded):[$^{13}C_6$]Arg (*m/z* 915.4; shaded) doublet as representative of all Gi-α3 peptide doublets from cells treated with 5 mM MβCD (A) or bSMase (B) for 2 h. The peak area ratios for all of the Gi-α3 peptide doublets from each treatment were calculated and are shown in the insets as means ± SEM.

nine to proline, which would produce [$^{13}C_5$]proline in cells supplemented with [$^{13}C_6$]Arg (32). Although this is not necessarily problematic for quantitation by SILAC, we observed no conversion of [$^{13}C_6$]Arg to [$^{13}C_5$]proline in either primary SCs or the S16 immortalized SCs.

The lower analytic limits for quantitation by SILAC were found to be an ~25% change in protein abundance. However, it should be noted that accurate quantitation of changes of this magnitude is facilitated by a high signal-to-noise ratio and is strengthened by quantifying as many peptide doublets as possible. Although the use of both [$^{13}C_6$]Arg and [$^{13}C_6$]lysine would further increase the number of peptide doublets available for quantitation (33), it has been our experience that lysine-containing peptides are poorly represented in the MALDI-TOF spectra, as has been reported previously (34). Collectively, these results provide the first evidence that SILAC analysis is feasible using either primary or immortalized SCs.

Overall, our MALDI-TOF analysis reproducibly identified and quantified 10 bona-fide caveolar proteins over the course of several different cell preparations and treatments (Table 2). Most of these proteins have been identified previously as lipid raft proteins based upon their 7.5- to10-fold decrease in association with CEMs after a 95% depletion of cholesterol using MβCD (25). Surprisingly, this level of cholesterol depletion resulted in only a 3-fold decrease in Cav-1 (25). Although bSMase treatment decreased cholesterol levels by 25–50% within 2 h, the relative abundance of Cav-1 decreased by 25% only after 8 h. On the other hand, ceramide-induced cholesterol depletion correlated with greater changes in the relative abundance of the β-subunit of ATP synthase and 5′-nucleotidase but had little effect on altering the association of flotillins or G-proteins with CEMs. Overall, it was quite surprising that a loss of 25–50% of the cholesterol content of the CEMs did not generate greater changes in the protein content of the membranes. Because ceramide-rich domains form highly ordered physical states in membranes and compete with cholesterol for association with rafts (7), it is possible that ceramide may substitute, in part, for the loss of cholesterol and protect some proteins from exiting the CEMs. The ability of Cav-1 to bind cholesterol may render this protein slightly more susceptible to exiting from the CEMs as ceramide displaces cholesterol. To examine this possibility further, we attempted to identify the receptor for the hedgehog proteins, Patched. Patched is expressed in SCs (35), is responsive to changes in cholesterol levels, binds to Cav-1, and localizes to lipid rafts (36). However, the identification of the rat homolog of Patched from the mouse or human protein sequences was not of high enough probability to allow a confident identification.

Finally, although bSMase is a pharmacological tool for increasing ceramide, the magnitude of the increase in ceramide is well within a range that is often produced by agonists or cell stress. Our observed loss of cholesterol from the CEMs, and its effect on the abundant structural proteins, may therefore be representative of physiological changes in these domains after the activation of plasma membrane SMases. However, the lipid and protein composition of lipid rafts is not necessarily identical between different cell types, and this may influence the rate of cholesterol and/or protein displacement induced by ceramide generation. Additionally, one must also consider that agonists also activate other sphingolipid-metabolizing enzymes (37) that may contribute to regulating the ceramide content and protein composition of lipid rafts.

In summary, our work suggests that both ceramide production and the loss of cholesterol from lipid rafts contribute to changes in the protein composition of these specialized membrane microdomains. Additionally, we demonstrate the feasibility of using SILAC in both immortalized and primary SCs to provide a quantitative proteomic approach to investigate signal transduction events in these cells. The application of SILAC analysis in the identification and quantification of changes in both protein abundance and protein phosphorylation (38) provides a useful tool for characterizing the effect of ceramide signaling on cellular or organellar proteomes.

This work was supported by grants from the American Diabetes Association, the National Institutes of Health (NS-38154), and a J. R. & Inez W. Jay Biomedical Research Grant. The authors thank Dr. Todd Williams for his advice and many useful discussions and Dr. D. Mikol for the S16 immortalized SCs.

REFERENCES

1. Simons, K., and D. Toomre. 2000. Lipid rafts and signal transduction. *Nat. Rev. Mol. Cell Biol.* **1:** 31–39.
2. Pike, L. J., X. Han, K. N. Chung, and R. W. Gross. 2002. Lipid rafts are enriched in arachidonic acid and plasmenylethanolamine and their composition is independent of caveolin-1 expression: a quantitative electrospray ionization/mass spectrometric analysis. *Biochemistry.* **41:** 2075–2088.
3. Masserini, M., P. Palestini, and M. Pitto. 1999. Glycolipid-enriched caveolae and caveolae-like domains in the nervous system. *J. Neurochem.* **73:** 1–11.
4. Razani, B., T. P. Combs, X. B. Wang, P. G. Frank, D. S. Park, R. G. Russell, M. Li, B. Tang, L. A. Jelicks, P. E. Scherer, et al. 2002. Caveolin-1-deficient mice are lean, resistant to diet-induced obesity, and show hypertriglyceridemia with adipocyte abnormalities. *J. Biol. Chem.* **277:** 8635–8647.
5. Brown, D. A., and E. London. 1998. Structure and origin of ordered lipid domains in biologic membranes. *J. Membr. Biol.* **164:** 103–114.
6. Massey, J. B. 2001. Interaction of ceramides with phosphatidylcholine, sphingomyelin and sphingomyelin/cholesterol bilayers. *Biochim. Biophys. Acta.* **1510:** 167–184.
7. London, M., and E. London. 2004. Ceramide selectively displaces cholesterol from ordered lipid domains (rafts): implications for lipid raft structure and function. *J. Biol. Chem.* **279:** 9997–10004.
8. Ito, J. I., Y. Nagayasu, and S. Yokoyama. 2000. Cholesterol-sphingomyelin interaction in membrane and apolipoprotein-mediated cellular cholesterol efflux. *J. Lipid Res.* **41:** 894–904.
9. Ong, S. E., B. Blagoev, I. Kratchmarova, D. B. Kristensen, H. Steen, A. Pandey, and M. Mann. 2002. Stable isotope labeling by amino acids in cell culture, SILAC, as a simple and accurate approach to expression proteomics. *Mol. Cell. Proteomics.* **1:** 376–386.
10. Blagoev, B., I. Kratchmarova, S. E. Ong, M. Nielsen, L. J. Foster, and M. Mann. 2003. A proteomics strategy to elucidate functional protein-protein interactions applied to EGF signaling. *Nat. Biotechnol.* **21:** 315–318.
11. Everley, P. A., J. Krijgsveld, B. R. Zetter, and S. P. Gygi. 2004. Quantitative cancer proteomics: stable isotope labeling with amino acids

in cell culture (SILAC) as a tool for prostate cancer research. *Mol. Cell. Proteomics.* **3:** 729–735.
12. Tan, W., S. Rouen, K. M. Barkus, Y. S. Dremina, D. Hui, J. A. Christianson, D. E. Wright, S. O. Yoon, and R. T. Dobrowsky. 2003. Nerve growth factor blocks the glucose-induced down-regulation of caveolin-1 expression in Schwann cells via p75 neurotrophin receptor signaling. *J. Biol. Chem.* **278:** 23151–23162.
13. Goda, S., J. Hammer, D. Kobiler, and R. H. Quarles. 1991. Expression of the myelin-associated glycoprotein in cultures of immortalized Schwann cells. *J. Neurochem.* **56:** 1354–1361.
14. Bilderback, T. R., R. J. Grigsby, and R. T. Dobrowsky. 1997. Association of $p75^{NTR}$ with caveolin and localization of neurotrophin-induced sphingomyelin hydrolysis to caveolae. *J. Biol. Chem.* **272:** 10922–10927.
15. Bligh, E. G., and W. J. Dyer. 1959. A rapid method of total lipid extraction and purification. *Can. J. Biochem. Physiol.* **37:** 911–917.
16. Dobrowsky, R. T., and R. N. Kolesnick. 2001. Analysis of sphingomyelin and ceramide levels and the enzymes regulating their metabolism in response to cell stress. *Methods Cell Biol.* **66:** 135–165.
17. Pike, L. J., and J. M. Miller. 1998. Cholesterol depletion delocalizes phosphatidyl-inositol bisphosphate and inhibits hormone-stimulated phosphatidylinositol turnover. *J. Biol. Chem.* **273:** 22298–22304.
18. Pandey, A., J. S. Andersen, and M. Mann. 2000. Use of mass spectrometry to study signaling pathways. *Sci. STKE.* Accessed May 16, 2005 at http://www.stke.org/cgi/content/full/OC_sigtrans:2000/37/pl1.
19. Ong, S. E., L. J. Foster, and M. Mann. 2003. Mass spectrometric-based approaches in quantitative proteomics. *Methods.* **29:** 124–130.
20. Gehrmann, M. L., Y. Hathout, and C. Fenselau. 2004. Evaluation of metabolic labeling for comparative proteomics in breast cancer cells. *J. Proteome Res.* **3:** 1063–1068.
21. Steen, H., and M. Mann. 2004. The ABC's (and XYZ's) of peptide sequencing. *Nat. Rev. Mol. Cell Biol.* **5:** 699–711.
22. Olsen, J. V., S. E. Ong, and M. Mann. 2004. Trypsin cleaves exclusively C-terminal to arginine and lysine residues. *Mol. Cell. Proteomics.* **3:** 608–614.
23. Murata, M., J. Peranen, R. Schreiner, F. Wieland, T. V. Kurzchalia, and K. Simons. 1995. VIP21/caveolin is a cholesterol binding protein. *Proc. Natl. Acad. Sci. USA.* **92:** 10339–10343.
24. Fielding, C. J., and P. E. Fielding. 2003. Relationship between cholesterol trafficking and signaling in rafts and caveolae. *Biochim. Biophys. Acta.* **1610:** 219–228.
25. Foster, L. J., C. L. De Hoog, and M. Mann. 2003. Unbiased quantitative proteomics of lipid rafts reveals high specificity for signaling factors. *Proc. Natl. Acad. Sci. USA.* **100:** 5813–5818.
26. Chatenay-Rivauday, C., Z. P. Cakar, P. Jeno, E. S. Kuzmenko, and K. Fiedler. 2004. Caveolae: biochemical analysis. *Mol. Biol. Rep.* **31:** 67–84.
27. Al Makdissy, N., M. Younsi, S. Pierre, O. Ziegler, and M. Donner. 2003. Sphingomyelin/cholesterol ratio: an important determinant of glucose transport mediated by GLUT-1 in 3T3-L1 preadipocytes. *Cell. Signal.* **15:** 1019–1030.
28. Subbaiah, P. V., S. J. Billington, B. H. Jost, J. G. Songer, and Y. Lange. 2003. Sphingomyelinase D, a novel probe for cellular sphingomyelin: effects on cholesterol homeostasis in human skin fibroblasts. *J. Lipid Res.* **44:** 1574–1580.
29. Cremesti, A. E., F. M. Goni, and R. Kolesnick. 2002. Role of sphingomyelinase and ceramide in modulating rafts: do biophysical properties determine biologic outcome? *FEBS Lett.* **531:** 47–53.
30. Terova, B., R. Heczko, and J. P. Slotte. 2005. On the importance of the phosphocholine methyl groups for sphingomyelin/cholesterol interactions in membranes: a study with ceramide phosphoethanolamine. *Biophys. J.* **88:** 2661–2669.
31. Steen, H., B. Kuster, M. Fernandez, A. Pandey, and M. Mann. 2002. Tyrosine phosphorylation mapping of the epidermal growth factor receptor signaling pathway. *J. Biol. Chem.* **277:** 1031–1039.
32. Ong, S. E., I. Kratchmarova, and M. Mann. 2003. Properties of ^{13}C-substituted arginine in stable isotope labeling by amino acids in cell culture (SILAC). *J. Proteome Res.* **2:** 173–181.
33. Ibarrola, N., D. E. Kalume, M. Gronborg, A. Iwahori, and A. Pandey. 2003. A proteomic approach for quantitation of phosphorylation using stable isotope labeling in cell culture. *Anal. Chem.* **75:** 6043–6049.
34. Krause, E., H. Wenschuh, and P. R. Jungblut. 1999. The dominance of arginine-containing peptides in MALDI-derived tryptic mass fingerprints of proteins. *Anal. Chem.* **71:** 4160–4165.
35. Parmantier, E., B. Lynn, D. Lawson, M. Turmaine, S. S. Namini, L. Chakrabarti, A. P. McMahon, K. R. Jessen, and R. Mirsky. 1999. Schwann cell-derived desert hedgehog controls the development of peripheral nerve sheaths. *Neuron.* **23:** 713–724.
36. Karpen, H. E., J. T. Bukowski, T. Hughes, J. P. Gratton, W. C. Sessa, and M. R. Gailani. 2001. The sonic hedgehog receptor patched associates with caveolin-1 in cholesterol-rich microdomains of the plasma membrane. *J. Biol. Chem.* **276:** 19503–19511.
37. Bourteele, S., A. Hausser, H. Doppler, J. Horn-Muller, C. Ropke, G. Schwarzmann, K. Pfizenmaier, and G. Muller. 1998. Tumor necrosis factor induces ceramide oscillations and negatively controls sphingolipid synthases by caspases in apoptotic Kym-1 cells. *J. Biol. Chem.* **273:** 31245–31251.
38. Hinsby, A. M., J. V. Olsen, and M. Mann. 2004. Tyrosine phosphoproteomics of FGF signaling—a role for insulin receptor substrate-4. *J. Biol. Chem.* **279:** 46438–46447.